Human Molecular Genetics, 2011, Vol. 20, No. 6 **1182–1196**
doi:10.1093/hmg/ddq563
Advance Access published on January 6, 2011

Reduced AKT/mTOR signaling and protein synthesis dysregulation in a Rett syndrome animal model

Sara Ricciardi[1,2,†], Elena M. Boggio[4,5,†], Stefano Grosso[3,6,†], Giuseppina Lonetti[7,†], Greta Forlani[8], Gilda Stefanelli[1,2], Eleonora Calcagno[4], Noemi Morello[4], Nicoletta Landsberger[2,8], Stefano Biffo[3,6], Tommaso Pizzorusso[5,7], Maurizio Giustetto[4,*] and Vania Broccoli[1,2,*]

[1]Stem Cells and Neurogenesis Unit, Division of Neuroscience, [2]San Raffaele Rett Research Center, Division of Neuroscience and [3]Laboratory of Molecular Histology and Cell Growth, Division of Oncology, San Raffaele Scientific Institute, 20132 Milano, Italy, [4]Department of Anatomia, Farmacologia e Medicina Legale, Università di Torino and National Institute of Neuroscience-Italy, Turin, Italy, [5]CNR, Neuroscience Institute Pisa, Pisa, Italy, [6]DISAV, University of Eastern Piedmont, 15100 Alessandria, Italy, [7]Department of Psicologia, Università di Firenze, Firenze, Italy and [8]Laboratory of Genetic and Epigenetic Control of Gene Expression, Department of Structural and Functional Biology, University of Insubria, 21052 Busto Arsizio, VA, Italy

Received October 19, 2010; Revised and Accepted December 27, 2010

Rett syndrome (RTT) is a neurodevelopmental disorder with no efficient treatment that is caused in the majority of cases by mutations in the gene methyl-CpG binding-protein 2 (*MECP2*). RTT becomes manifest after a period of apparently normal development and causes growth deceleration, severe psychomotor impairment and mental retardation. Effective animal models for RTT are available and show morphofunctional abnormalities of synaptic connectivity. However, the molecular consequences of MeCP2 disruption leading to neuronal and synaptic alterations are not known. Protein synthesis regulation via the mammalian target of the rapamycin (mTOR) pathway is crucial for synaptic organization, and its disruption is involved in a number of neurodevelopmental diseases. We investigated the phosphorylation of the ribosomal protein (rp) S6, whose activation is highly dependent from mTOR activity. Immunohistochemistry showed that rpS6 phosphorylation is severely affected in neurons across the cortical areas of *Mecp2* mutants and that this alteration precedes the severe symptomatic phase of the disease. Moreover, we found a severe defect of the initiation of protein synthesis in the brain of presymptomatic *Mecp2* mutant that was not restricted to a specific subset of transcripts. Finally, we provide evidence for a general dysfunction of the Akt/mTOR, but not extracellular-regulated kinase, signaling associated with the disease progression in mutant brains. Our results indicate that defects in the AKT/mTOR pathway are responsible for the altered translational control in *Mecp2* mutant neurons and disclosed a novel putative biomarker of the pathological process. Importantly, this study provides a novel context of therapeutic interventions that can be designed to successfully restrain or ameliorate the development of RTT.

INTRODUCTION

Rett syndrome (RTT; MIM312750) is a pediatric neurological progressive disorder leading to severe mental retardation, psychomotor impairment and autistic behavior that affects about 1:10 000 girls worldwide (1–3). Children with RTT have apparently normal development until 6 months of life, after which they undergo a rapid regression marked by a

*To whom correspondence should be addressed at: San Raffaele Scientific Institute, Via Olgettina 58, 20132 Milan, Italy.
Tel: +39 02 26434616; Fax: +39 02 26434621; E-mail: broccoli.vania@hsr.it (V.B.); Department of Anatomia, Farmacologia e Medicina Legale, Università di Torino and National Institute of Neuroscience-Italy, Turin, Italy (M.G.).
†These authors contributed equally to this work.

deceleration of head growth, the onset of stereotyped hand movements, irregular breathing and seizures (4). Loss-of-function mutations in the X-linked methyl-CpG-binding protein 2 (*MECP2*) gene, a transcriptional regulator that acts through epigenetic mechanisms on chromatin structure (5), cause the 95% of RTT cases. Importantly, mutations of this gene are also found in patients with other neurological conditions such as Angelman-like syndrome, motor and learning disabilities, seizures, bipolar disease, juvenile-onset schizophrenia, neonatal encephalopathy and autism (2,6,7). The finding that in mice targeted the mutation of *Mecp2* in the central nervous system may produce a phenotype similar to the whole-body mutation has suggested that impairment of MeCP2 function in the brain is crucial for the pathogenesis of the disease (8,9). Indeed, the analysis of the available animal models for RTT has indicated that altered MeCP2 levels in neurons cause morphological defects in both dendritic complexity, spine number as well as alterations in synaptic transmission and plasticity (10–16). These results have suggested a model for the etiopathogenesis of RTT in which the behavioral alterations induced by the *Mecp2* mutation could depend on the modifications of brain synaptic organization. However, the molecular events leading from the disruption of *Mecp2* expression in the brain to the alterations of neuronal circuits are yet not known.

There is mounting evidence showing that aberrant neuronal protein synthesis as one underlying cause of the clinical features of autism spectrum disorders (17,18). Alterations of signaling cascades involved in the regulation protein synthesis, such as the mammalian target of rapamycin (mTOR) and phosphoinositide 3-kinase (PI3K) pathways, have been involved in neurodevelopmental diseases associated with severe mental retardation (19,20) such as Fragile X (21), tuberous sclerosis (22) and Phelan-McDermid syndrome (23). Interestingly, the regulation of protein synthesis via the mTOR/PI3K pathway is crucially involved in synaptic function, structure and plasticity (20,24–26). In post-mitotic neurons, mTOR activity and its downstream targets can control the size of the neuronal cell soma, axon pathfinding and regeneration, dendrite arborization, dendritic spine morphology and synaptic plasticity (20,25). Intriguingly, all these aspects are altered in *Mecp2* mutants. These changes are not accompanied, surprisingly, by important changes in the transcriptome (1,27,28), suggesting that *Mecp2* may subtly act at the post-transcriptional level. In spite of it, studies describing the efficacy of protein synthesis or the translation-related intracellular signaling in RTT are not yet available.

In this study, we investigate whether the activation of ribosomal protein (rp) S6, a component of the 40S ribosomal subunit, is normal during the post-natal brain development of *Mecp2* mutant mice. In particular, we analyze the modifications occurring at Ser235/236 and Ser240/244. These residues can be phosphorylated by both the extracellular-regulated kinase (ERK) and the mTOR/PI3K pathway and correlate with cellular translational rates (29–31). Moreover, to test the hypothesis that translational deficits may be a cause of RTT neurological dysfunctions, we looked at polysomal complexity and polysome-associated mRNAs in the brain of *Mecp2* mutants. Finally, we analyze the contribution of intracellular upstream signaling to dissect out the mechanism regulating protein synthesis in neurons completely lacking *Mecp2*.

RESULTS

Pervasive hypophosphorylation of rpS6 in *Mecp2*$^{-/y}$ brains precedes symptoms manifestation

mTOR/PI3K-dependent protein synthesis in neurons is crucial for the organization of neuronal and synapse structures (e.g. dendrites and dendritic spines) as well as for synaptic plasticity (24–26). In addition, dendritic protein synthesis induced by activation and plasticity of synaptic connections requires the action of ERK-dependent signaling (24,32,33). To address weather possible defects of these intracellular pathways might occur in the brain of *Mecp2* knock-out (KO) mice (*Mecp2*$^{tml.1Jae}$) (8), we examined the immunolocalization of phosphorylated (p) rpS6, a converging target of both ERK and mTOR/PI3K activity (31). We analyzed the localization of activated rpS6 in the primary sensory (S1) cortex and in the CA1 region of the hippocampus, where neuronal and synaptic alterations have previously been found in mice models of RTT (10,12,15,34–37). The analysis was performed in *Mecp2*$^{-/y}$ mice at 8 weeks of age (P56) showing clear symptomatic signs (i.e. locomotor impairments, hind limb clasping, perseverative scratching and breathing irregularities). Sections were probed with two specific antibodies. The first recognizes rpS6 only when is activated at Ser235/236, two residues that can be phosphorylated by both ERK and mTOR/PI3K activities. The second antibody recognizes the activated form of rpS6 at Ser240/244 sites, a modification that can be induced by the action of the mTOR/PI3K pathway and is ERK-independent.

As illustrated in Figure 1A, we observed a robust decrease in p-rpS6 immunoreactivity throughout the S1 cortex of *Mecp2* mutants compared with wild-type (WT) littermates. In general, rpS6 activation was more intense in layer 5 of the cortex of WT animals. A close inspection of the immunolabeled sections revealed that in individual cortical neurons, rpS6 can be activated both in the soma and in the most proximal portion of the apical dendrite. As can be inferred in Figure 1A insets, rpS6 staining showed differences among the cells. Remarkably, quantification of the immunosignal intensity (Fig. 1D), calculated as optical density (OD) values of the peroxidase staining, confirmed a significant decrease in rpS6 activation at both Ser235/236 and Ser240/244 in the *Mecp2* mutants. We found a 32.2% reduction in p-rpS6 (Ser235/236) activation throughout the cortex of KO mice in comparison with WT littermates ($n = 3$, $P < 0.005$), whereas the activation of p-rpS6 (Ser240/244) was 30.2% less in the mutants than in control animals ($n = 3$, $P < 0.05$). In contrast, we detected neither differences in localization (Fig. 1A) nor significant changes in immunolabeling intensity (Fig. 1B) for the total rpS6 protein between WT and *Mecp2*$^{-/y}$ mice. Thus, because of reduced phosphorylation, rpS6 cannot properly function in symptomatic *Mecp2* KO male mice.

To address whether dysfunctional rpS6 phosphorylation in the cortex may either anticipate or correlate with the

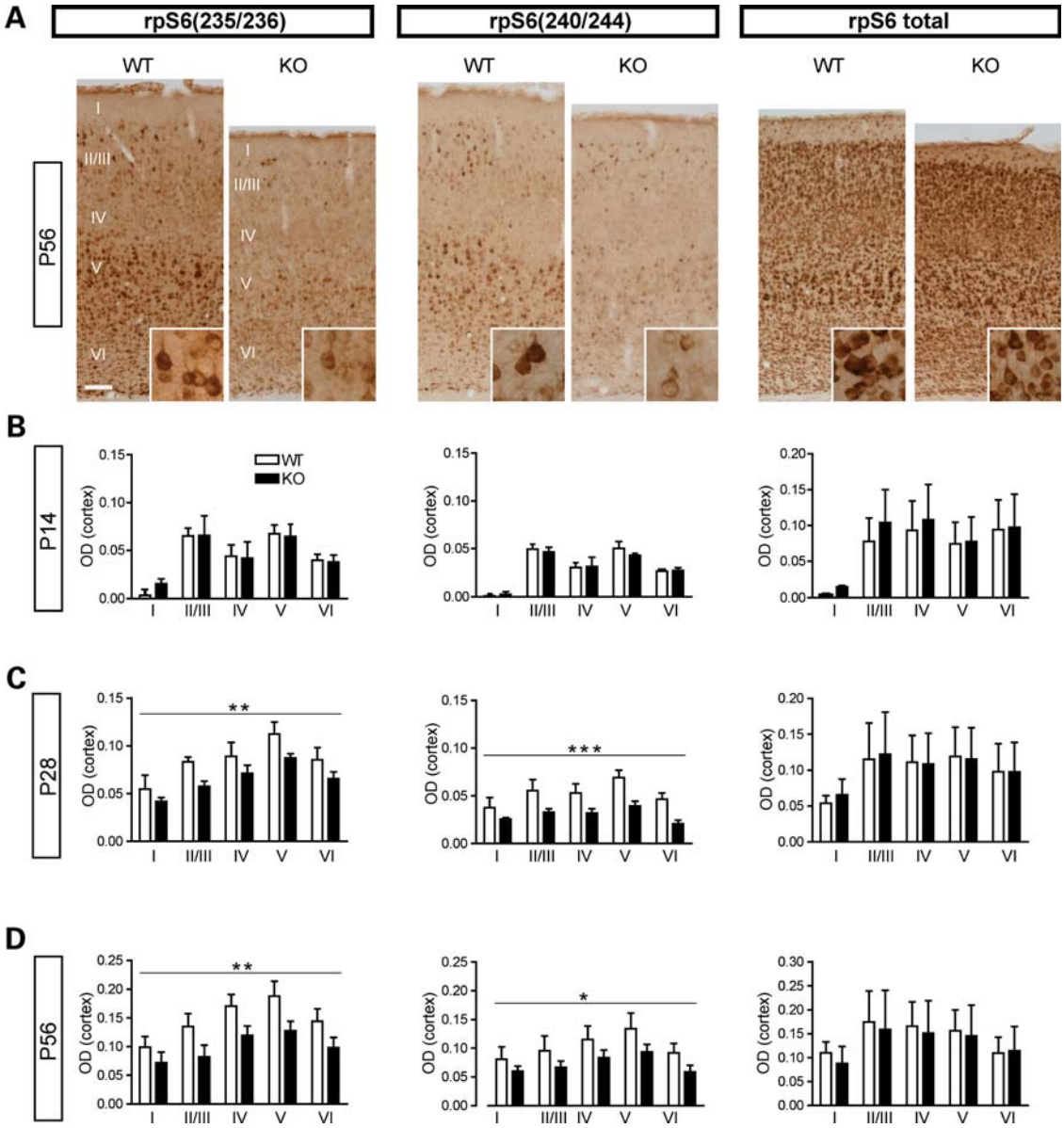

Figure 1. The loss of MeCP2 leads to defective rpS6 activation in the S1 cortex of adult mice. (**A**) Representative micrographs of S1 cortex cryosections of symptomatic mice at 56 days of age showing the reduction in both p-rpS6 (Ser235/236) and p-rpS6 (Ser240/244) immunoreactivity in MeCP2 KO animals. Total rpS6 immunoreactivity is unchanged between WT and control animals. Insets show higher magnification views of the immunolabeling in layer V neurons. Reduced cortical thickness shown by MeCP2 KO sections compared with WT controls is representative of a previously reported morphological alteration affecting mutants (61) and is not due to fixation artifacts or a mismatch of cortical areas that were examined in this study. (**B**–**D**) Histograms illustrate the evaluation of rpS6 phosphorylation levels as well as total rpS6 expression in each layer (I–VI) of the S1 cortex. Data are expressed as the mean OD values of the immunoperoxidase labeling. (B) At P14, labeling intensity for both the activated and the total rpS6 shows no statistically significant variations between KO mice and WT littermates. The decrease in p-rpS6 (Ser235/236 and Ser240/244) labeling intensity is highly significant and is spread throughout the cortical layers of P28 (C) and P56 (D) KO mice compared with WT littermates. Total rpS6 expression is not altered in these animals. Data are expressed as the mean ± sem. $^{*}P < 0.05$, $^{**}P < 0.01$, $^{***}P < 0.001$ (scale bar, 100 μm).

disease progression, we next examined KO animals at earlier post-natal ages (i.e. P14 and P28). As illustrated in Figure 1C, at P28, i.e. before the appearance of evident locomotor deficits and hind limb clasping in *Mecp2* KO mice, mutants show a significative reduction in p-rpS6 immunoreactive signals (p-rpS6-Ser235/236: 23.6% reduction in KO mice versus WT littermates, $n = 3$ WT and KO, $P < 0.005$; p-rpS6-Ser240/244: 41.4% reduction in KO mice versus WT littermates, $n = 3$ WT and KO, $P < 0.001$). Intriguingly, at an earlier post-natal developmental stage (P14), when mutants are asymptomatic, KO mice showed WT levels of rpS6 activation (Fig. 1B). At this early post-natal developmental stage, we detected no differences in rpS6 immunostaining intensity for any of the phosphorylation sites throughout the cortical layers. Quantitative evaluation of rpS6 immunostaining showed no differences between the two genotypes at

both P14 and P28 (Fig. 1C and D). These data indicate that after a period of putative normal activity, rpS6 becomes hypofunctional in correlation with the onset of the symptoms.

To determine whether rpS6 phosphorylation may be similarly affected in other brain areas, we, next, performed a similar immunohistochemical analysis of p-rpS6 localization in the CA1 hippocampal area of *Mecp2* mutants at the three ages examined previously. Interestingly, although CA1 pyramidal neurons in MeCP2 KO mice showed less rpS6 activation than WT animals (Supplementary Material, Fig. S1) the effect was less dramatic than what we observed in the S1 cortex. In particular, we found that there is a significant decrease in rpS6 activation on Ser240/244 in P28 KO mice (Supplementary Material, Fig. S1D; OD WT: 0.16 ± 0.02; OD KO: 0.08 ± 0.01; $n = 3$ WT and KO, $P < 0.05$).

It has been recently shown that glial cells lacking MeCP2 may cause defects in the dendritic morphology and complexity of co-coltured MeCP2-positive neurons thus implying a critical role of the glia in the neurological alterations associated with RS (38). To explore whether the rpS6 phosphorylation changes observed in *Mecp2* (P28) mutants are associated with alterations occurring also in glial cells we analyzed rpS6 phosphorylation in dually labeled brain sections with antibodies against GFAP or NeuN. As illustrated in Figure S2, the number of $GFAP^+$ glial cells was very low throughout the layers of the S1 cortex in both WT and mutant animals. Moreover, virtually no co-localization between $GFAP^+$ cells and p-rpS6-Ser235/236 or p-rpS6-Ser240/244 immunosignal was detectable in sections from both genotypes (Supplementary Material, Fig. S2A and B) indicating that rpS6 shows extremely low levels of activation in glial cells. In contrast, we found that practically all p-$rpS6^+$ cortical cells were clearly co-labeled with NeuN antibody (Supplementary Material, Fig. S2A and B). Importantly, the specific neuronal rpS6 activation was also observed in labeled sections from the CA1 area of the hippocampus (Supplementary Material, Fig. S2A and B). Indeed, while p-rpS6 immunofluorescence was not detectable in $GFAP^+$ cells, $NeuN^+$ CA1 pyramidal neurons were co-labeled with the p-rpS6 antibodies. Thus, these data suggest that the consequences of rpS6 hypofunction in the brain of *Mecp2* mutants are primarily attributable to neuronal activation defects.

In a second approach, we independently quantify the reduction in the rpS6 phosphorylation levels at Ser235/236 and Ser240/244 by western blot analysis carried out on three isolated brain regions, i.e. cerebral cortex, hippocampus and cerebellum. Phosphorylated rpS6 levels were confirmed to be strongly decreased in cortex and cerebellum and, to a lesser extent, in the hippocampus of brains lacking *Mecp2*, whereas total rpS6 levels were unaltered (cortex: p-rpS6-Ser235/236, reduced to $55.1 \pm 11.1\%$ of WT levels, $n = 9$, $P = 0.001$; p-rpS6-Ser240/244, reduced to $35.2 \pm 10.7\%$ of WT levels, $N = 8$ $P = 0.009$; cerebellum: p-rpS6-Ser235/236, reduced to $31.9 \pm 6.5\%$ of WT levels, $n = 6$, $P = 0.005$; p-rpS6-Ser240/244, reduced to $29.5 \pm 12.6\%$ of WT levels, $n = 4$, $P = 0.002$; hippocampus: p-rpS6-Ser235/236, reduced to $56.2 \pm 5.6\%$ of WT levels, $n = 4$, $P = 0.02$; p-rpS6-S240/244, reduced to $68.9 \pm 16.6\%$ of WT levels, $n = 11$, $P = 0.15$; Fig. 2A–C). In general, we found a decrease in phosphorylation in Ser240/244 and Ser235/236, except for the hippocampus, where the reduction in Ser240/244 phosphorylation was not statistically significant thus suggesting that rpS6 function might be differentially affected in specific neuronal circuits by the absence of *Mecp2*.

Protein synthesis is severely affected in *Mecp2* mutant brains

The phosphorylation of rpS6 is regulated by the ERK (31) and mTOR pathways with the last being prominent in most cells, and highly sensitive to mTOR inhibition (39). Moreover, rpS6 phosphorylation correlates with the activation of the protein synthesis apparatus (30).

With this in mind, we decided to analyze protein synthesis in *Mecp2* mutant mice at P56. Neuropathological signs are already developed at this stage exemplified by motor unbalance, learning impairments as well as cognitive deficits and anxious behavior (37) are already developed.

To have a read-out of protein synthesis, incorporation of ^{35}S-methionine into new proteins was examined on *in vitro* cultured brain slices of WT ($n = 3$) and MeCP2 mutant brains ($n = 3$). This metabolic labeling showed a trend in reduction in methionine incorporation ($P = 0.06$) in the mutants (Supplementary Material, Fig. S3), prompting us to analyze the specific reduction in initiation of translation by polysomal profiles.

Cytoplasmic cell extracts from *Mecp2* mutant and WT brain lysates were prepared and fractioned on a sucrose gradient. Figure 3A shows cell extracts profiles in which the polysomal fraction is evidently reduced in two different MeCP2 mutants (red line) when compared with WT (black line) brains (WT, $n = 3$; KO, $n = 3$). Therefore, the overall pool of active translating polyribosomes is abnormally diminished in mutant brains where the disease has progressed. Indeed, densitometric scanning of the P56 brain polysomal profiles (Fig. 3B) showed a significant decrease in the area of ribosomal peaks in the polysome fraction of *Mecp2* null mice with respect to WT littermates (decrease of $8 \pm 0.1\%$ of WT, $n = 3$, $P < 0.05$). Consistently, there was an increase in the area of ribosomal peaks in the mRNA-free part of the gradient in *Mecp2* null mice with respect to WT controls (increase of $7.9 \pm 0.08\%$ of WT, $n = 3$, $P < 0.05$).

This dysfunction of initiation of the translation rate might be caused by the general compromised state of the mutants at this late phase of the disease. In alternative, this defect might be an early event in the disease evolution that, nonetheless, remains detectable even at late stages of the pathology. To discriminate between these two possibilities, we performed polysomal profiles in young *Mecp2* null animals at a presymptomatic stage (P26). Noteworthy, cell extracts profiles present a notable reduced polysomal fraction when comparing *Mecp2* null with WT brains (WT, $n = 3$; KO, $n = 3$) (Fig. 3C). The densitometric scanning of the P26 brain polysomal profiles (Fig. 3D) showed a significant decrease in the area of ribosomal peaks in the polysome fraction of *Mecp2* null mice with respect to WT littermates (decrease of $7.6 \pm 0.04\%$ of WT, $n = 3$, $P < 0.01$). Consistently, there was an increase in the area of ribosomal peaks in the mRNA-free part of the gradient in *Mecp2* null mice with respect to WT controls (increase of $7.6 \pm 0.03\%$ of WT, $n = 3$, $P < 0.01$).

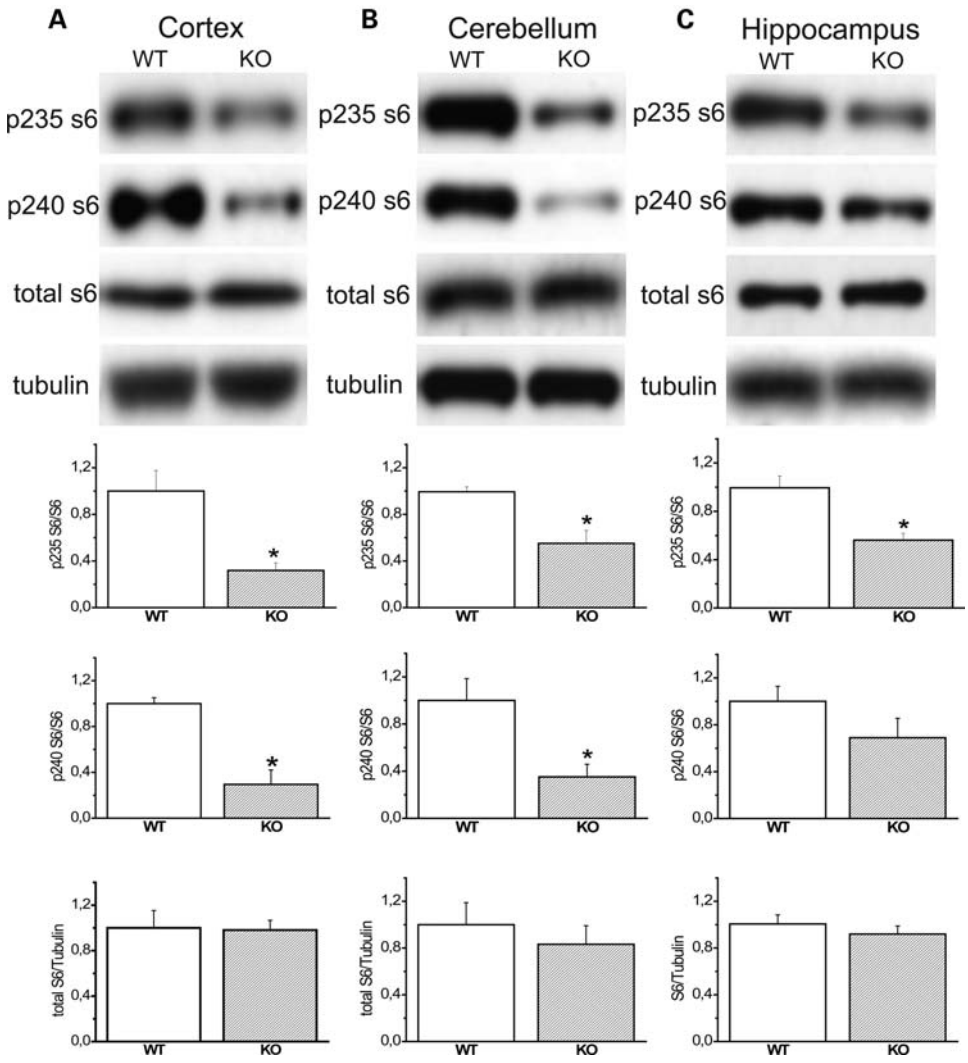

Figure 2. S6 phosphorylation is reduced in the cortex, cerebellum and hippocampus of MeCP2$^{-/y}$ animals. Representative western blots (top) and summary data (bottom) showing p-rpS6 and total pS6 in whole-cell lysates from the cortex (**A**), cerebellum (**B**) and hippocampus (**C**) of P56 MeCP2 KO and WT mice. Western blots were probed with antibodies to p-Ser235/236 S6, p-Ser240/244 S6 and total S6. Tubulin was included as a loading control. Blot quantitation revealed that the phosphorylation of S6 at Ser235/236 is reduced in cortex, cerebellum and hippocampus of MeCP2 KO animals. rpS6 Ser240/244 phosphorylation was significantly reduced in MeCP2 KO cortex and cerebellum but not in the hippocampus. No difference was present in total rpS6 expression. Error bars represent the standard error of the mean. $^{*}P < 0.05$.

In line with this finding, the amount of Rack1, a major component of translating ribosome, was mainly reduced in the fast sedimenting fractions (7–10) where polyribosomes are located in the MeCP2 null with respect to the control brain lysates (Fig. 3D). Conversely, at this same stage initiation of translation was found only minimally affected in the liver of MeCP2 mutant with respect to WT animals (WT, $n = 3$; KO, $n = 3$), a peripheral organ with an intense metabolic activity (Fig. 3B). These data provide a first indication that defects in the initiation of translational are an early sign of the disease that accompanies or even precedes the initial neurological impairment in the MeCP2 null mice.

A failure in initiation might have a general impact on global mRNA translation or, alternatively, might affect specific transcripts in particular. To address this issue, RNA was isolated from each fraction of the ribosomal profiles of P26 *Mecp2* mutant and WT brain lysates and transcript levels for a specific gene were assessed by quantitative RT-PCR (qRT-PCR). We selected two genes coding for molecules with a pivotal function in neuronal activity and plasticity such as CAMKIIα and PSD95. In addition, three genes not associated with a neuronal function were also analyzed (Rack1, hnRNP A2/B1 and GADPH). Finally, we assessed the levels of the 18S ribosomal RNA (rRNA) which is incorporated in 40S ribosomal subunit. In total agreement with polysomal profiles, in MeCP2 mutant brains, the 18S rRNA was reduced in the polysome fraction and enriched in the mRNA-free part of the gradient (Fig. 4A). A similar trend was observed for CAMKIIα and PSD-95 mRNAs as well as for Rack1, hnRNP A2/B1 and GADPH mRNAs (Fig. 4B–D). Indeed, polysomal incorporation of these transcripts was significantly lower in *Mecp2* null mice with respect to WT (Fig. 4B–D). This observation can be quantitatively expressed by the percentage of messenger on polysomes (PMP), which is calculated by dividing the sum of the

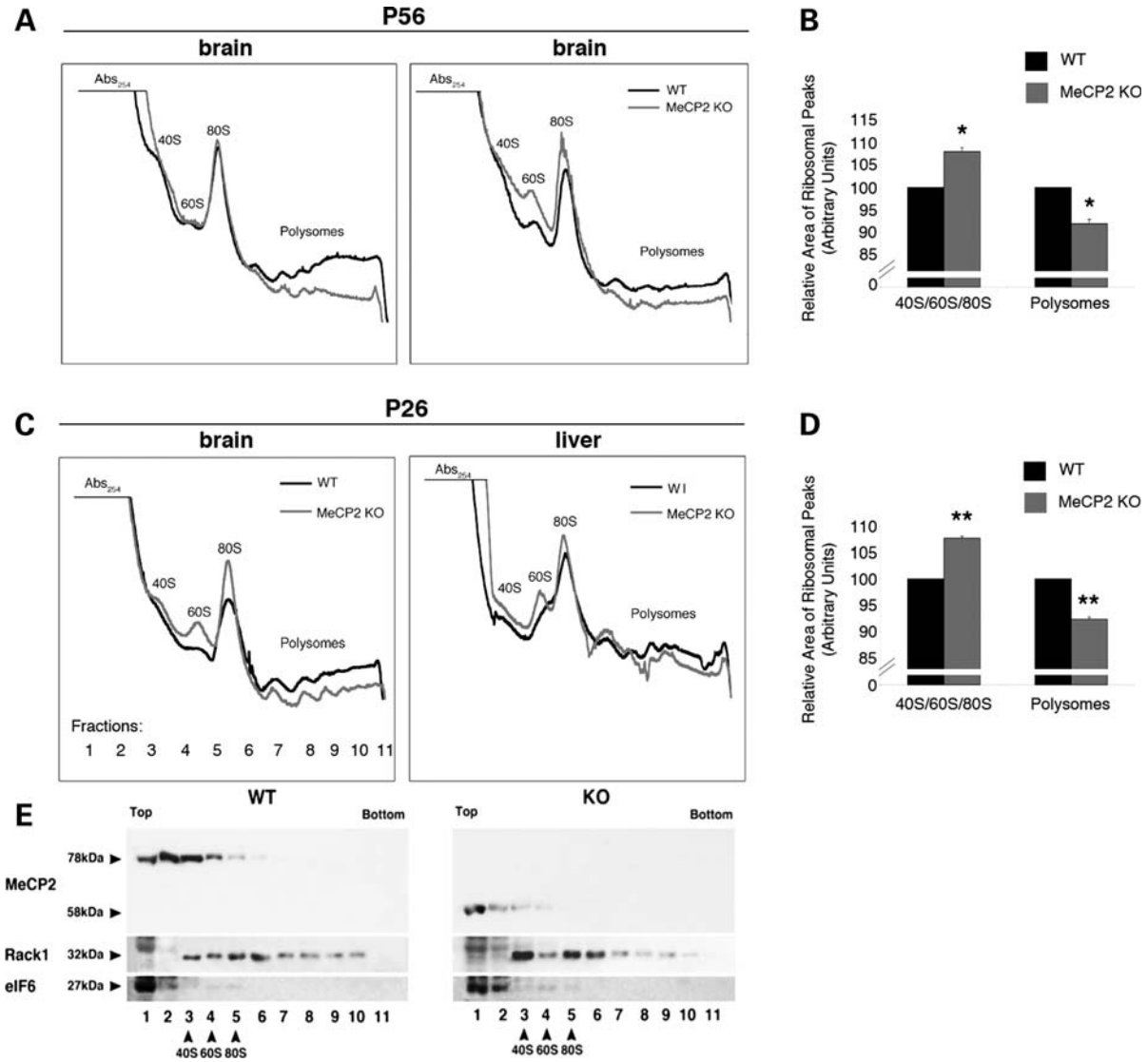

Figure 3. Initiation of translation is reduced in MeCP2$^{-/-}$ adult and young mice. (**A**) Polysomal profiles of P56 WT and MeCP2 KO mouse brain extracts. Cytoplasmic brain extracts derived from P56 WT and MeCP2 KO mice were fractionated on a 15–50% (w/v) linear sucrose gradient. Polysomal profiles show the difference in the initiation of translation between WT and MeCP2 null mice. Specifically, the increase in 80S and the decrease in polysomes peaks indicate that the level of translation in MeCP2 KO is decreased. (**B**) Densitometric scanning quantification of P56 brain polysomal profiles is presented in a bar graph. Error bars represent the standard deviations from the means. $^{*}P < 0.05$. (**C**) Polysomal profiles of P26 WT and MeCP2 null mouse brain extracts. Cytoplasmic brain extracts derived from P26 WT and MeCP2 KO mice were fractionated on a 15–50% (w/v) linear sucrose gradient. The same experiment was carried out on mouse liver, showing little or no difference in translation between WT and MeCP2 KO. (**D**) Densitometric scanning quantification of the relative area of ribosomal peaks of P26 brain polysomal profiles is presented in a bar graph. Error bars represent the standard deviations from the means. $^{**}P < 0.01$. (**E**) Fractions from polysomal profiles of P26 WT and MeCP2 null brains were collected, TCA concentrated and analyzed by SDS–PAGE. Proteins were probed for MeCP2, Rack1 (marker of 40S, 80S and translating ribosomes) and eIF6 (marker of free 60S).

quantitated signals of the last six fractions containing active polysomes by the sum of the 11 fractions. In the case of control tissues, the PMP value was over 60% for all six genes, whereas it got reduced to ~50% in *Mecp2* mutant brains (Fig. 4D). Taken together, these data demonstrate a comparable reduction in the translation rate of all the tested mRNAs.

AKT/mTOR signaling is perturbed in *Mecp2* mutant brain tissue

mRNA translation is a highly regulated process and represents the final target of diverse signaling pathways that sense both the stimuli from the external environment as well as the metabolic needs. Therefore, we decided to investigate any changes in diverse intracellular pathways involved in protein synthesis. It is well recognized that rpS6 is the major substrate of p70 S6 kinase (S6K) which promotes the phosphorylation of consecutive serine residues at the rpS6 C-terminal part and thereby stimulating protein translation (30). Activation of the p70 S6K depends on multiple phosphorylation events occurring in a hierarchical manner within the C-terminal autoinhibitory domain (40). Interestingly, the S6K phosphorylation levels were reduced in brain lysates of P48 *Mecp2* mutant with respect to WT

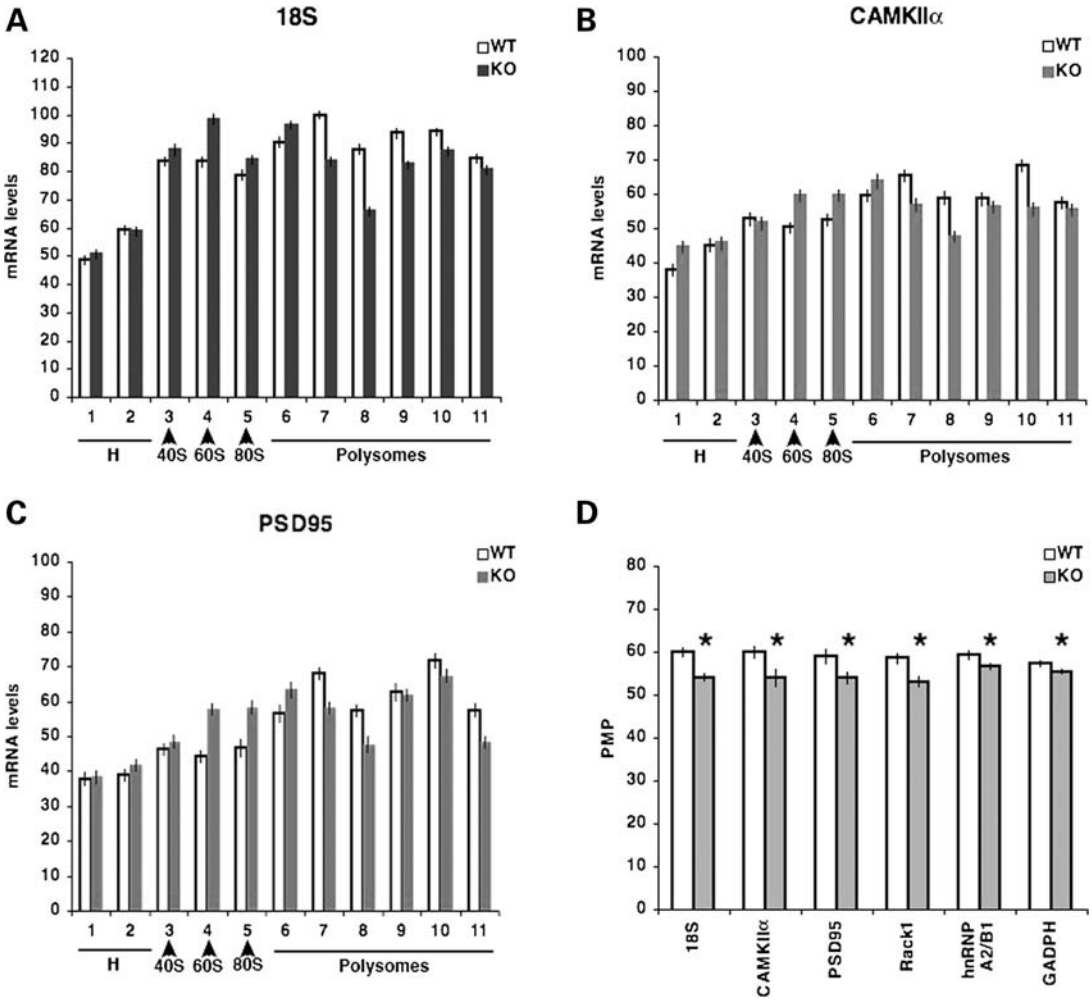

Figure 4. Polysomal incorporation of 18S rRNA as well as CAMKIIα, PSD95, Rack1, hnRNP A2/B1 and GADPH mRNAs is decreased in the absence of MeCP2. Cytoplasmic brain extracts derived from P26 WT and MeCP2 null mice were fractionated on a 15–50% (w/v) linear sucrose gradient. Each gradient was fractionated into 11 1-ml fractions, RNA was extracted from each fractions and qRT-PCR analyzes of total RNA in each fraction was carried out with primers specific for 18S, CAMKIIα PSD95, Rack1, hnRNP A2/B1 and GADPH. Results pooled into five groups: Hydrosol (H), 40S, 60S, 80S and polysomes. Error bars represent the standard deviations from the means ($n = 3$). $^{*}P < 0.05$ for KO versus WT by Student's *t*-test. 18S, CAMKIIα and PSD95 mRNA levels are significantly decreased in active polysomes from MeCP2 KO brain (**A**–**D**). These data suggest the decreased levels of mRNA translation in MeCP2 KO. (D) Histogram of PMP is reported. PMP was calculated by comparing the mRNA level of the fractions containing active polysomes with the mRNA level from all 11 fractions.

littermates (decrease of 35 ± 6% of WT; $n = 3$ WT and KO; $P < 0.05$) (Fig. 5A and B). In contrast, no appreciable change was detected in S6K protein abundance between *Mecp2* null and WT brain lysates (Fig. 5A and B).

A large body of evidence has shown that the rpS6-S6K pathway is tightly controlled by the mTOR kinase activity which integrates signals from mitogenic growth factors, nutrients, stress and cellular energy level to promote protein synthesis (41,42). Therefore, we examined the abundance and phosphorylation of mTOR at Ser2448, a biochemical indicator of mTOR activation (41), in *Mecp2* KO and WT brain lysates. The phosphorylation of mTOR at Ser2448 was reduced in whole-cell lysates of the brain of *MeCP2* mutant mice (decrease of 27 ± 7% of WT; $n = 3$ WT and KO; $P < 0.05$) relative to that of WT littermates (Fig. 5C and D). In contrast, the amount of the total mTOR protein was equivalent in both genotypes indicating a reproducible difference exclusively to its phosphorylated form (Fig. 5C and D). rpS6 is known to be also activated by the RAS-ERK signaling cascade through phosphorylation by the p90 ribosomal S6K exclusively in Ser235/236 (31). Thus, we examined the levels of the activation of Erk1/2 kinases in brains lacking *Mecp2*. No difference in ERK2 phosphorylation was observed in the same mice (94.4 ± 17% of WT levels, $n = 11$, $P = 0.56$) (Fig. 6A and B).

The findings reported thus far suggest a rather specific defect in mTOR signaling in the brain of *MeCP2* KO mice. At least two mTOR complexes exist, mTORc1, upstream of rpS6, and mTORc2. The phosphorylation status of S473 depends directly by mTORc2 activity and therefore represents an indication of the overall mTOR activity in the cell (43). Interestingly, we found a consistent reduction in AKT S473 phosphorylation in mutant *Mecp2* compared with WT P46 brain lysates (decrease to 45.7 ± 9.5% of WT levels, $n = 10$, $P = 0.037$) (Fig. 6C and D).

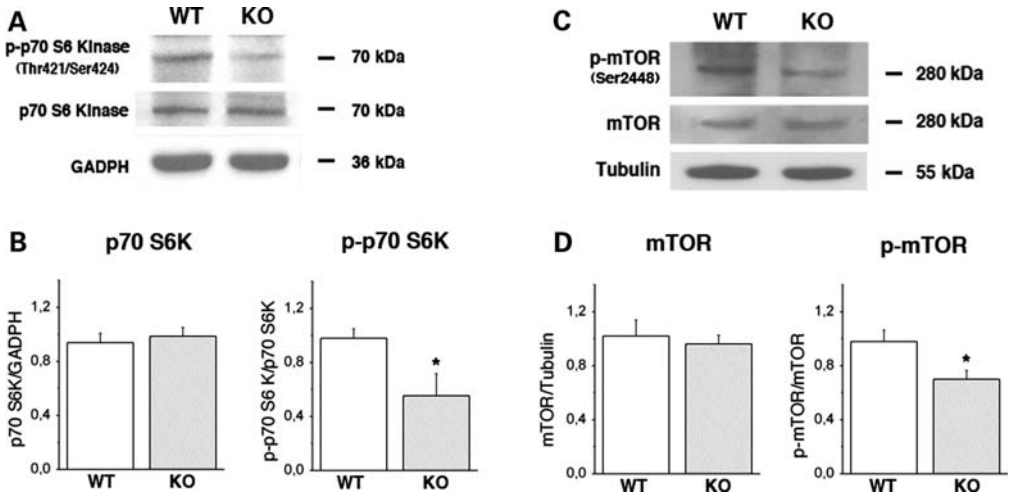

Figure 5. Suppression of mTOR signaling in MeCP2$^{-/y}$ mouse brain. (**A**) Brain lysates from P26 WT and MeCP2 null mice were separated by SDS–PAGE, and the phosphorylation of p70 S6K was analyzed by western blot. Western blots were probed with antibodies against p-Thr421/Ser424-p70 S6K and total p70 S6K. GADPH was included as a loading control. Western blot analysis revealed that the phosphorylation of p70 S6K is basally reduced in MeCP2 KO brain. (**B**) Densitometric scanning quantification of the relative abundance of p-p70 S6K is presented in a bar graph. The values correspond to the means of three independent experiments. Error bars represent the standard deviations from the means. (**C**) The same experiment as in (A) was carried out with antibodies to p-Ser2448-mTOR and total mTOR. Tubulin was included as a loading control. (**D**) Summary data showing the relative abundance of p-Ser2448-mTOR in whole-brain lysates from MeCP2 KO and WT mice. The values correspond to the means of three independent experiments. Error bars represent the standard deviations from the means. $^{*}P < 0.05$.

The difference in phospho-AKT appears to be attributable to alterations in basal activation state, because total AKT abundance did not differ significantly in mutant mice relative to WT littermates (Fig. 6A and B).

In overall, these results provide evidence for a general dysfunction of the AKT/mTOR signaling associated with the disease progression in *Mecp2* mutant brains.

MeCP2 is not a ribosomal resident protein

To assess any direct involvement of MeCP2 in controlling protein synthesis, we investigated its association with the ribosomal machinery. In polysomal profiles, MeCP2 was mainly localized in fractions 1–5 partially co-fractionating with ribosomal subunits 40S, 60S and 80S as tested by immunoblotting with two different antibodies on each fraction of the gradient (see Materials and Methods). To determine whether the co-sedimentation of MeCP2 with ribosomes is stable, we repeated ribosomal profiles after treating cell extracts with EDTA (30 mM) which causes complete dissociation of the translating ribosomes into subunits and the release of polyribosomal mRNPs. In this case, ribosomal-associated proteins no longer were collected from the fast-sedimenting gradient fractions, but were retrieved from the fractions at the top of the sucrose gradient (Supplementary Material, Fig. S4). In line with this, Rack1, a protein stable associated with ribosomes, after EDTA treatment was mostly located in the cellular soluble content confirming the expected outcome. Nevertheless, under these conditions, the MeCP2 sedimentation pattern was neither shifted into the lighter fractions nor changed in other evident ways (Supplementary Material, Fig. S4). These results indicate that MeCP2 is associated with high-weighted molecular complexes but it is not stably associated with ribosomal complexes.

Phosphorylation of rpS6 is abnormal in *Mecp2*$^{+/-}$ female mice

Mecp2$^{y/-}$ mutants are the most utilized animal model to evaluate harsh consequences of MeCP2 mutation. However, the greatest number of the affected RTT patients is MECP2-mutated heterozygote girls. *Mecp2*$^{+/-}$ female mice possess various phenotypic characteristics of RTT patients, such as locomotor and autonomic alterations, abnormal cognitive and emotional behavior as well as a relatively normal lifespan.

We thus analyzed if the phosphorylation of rpS6 is impaired in the brain of 10 months old female heterozygous mutants that showed clear signs of the pathology (i.e. tremors, reduced size and severe locomotor defects). As shown in Figure 7A, we found that the intensity of immunostaining for the phosphorylated forms of rpS6 (Ser235/236 and Ser240/244 sites) was drastically reduced in the brain of *Mecp2*$^{+/-}$ mutants compared with WT female animals of the same age. The decrease in p-rpS6 levels was observed throughout the layers of the S1 cortex and in the CA1 area of the hippocampus (Fig. 7A). Indeed, OD analysis of the immunolabeling intensity (Fig. 7B) showed a significant decrease in rpS6 activation at both Ser235/236 ($P < 0.001$) and Ser240/244 ($P < 0.001$) in the S1 cortex of MeCP2 heterozygous mutants. We found a 60.1% reduction in p-rpS6 (Ser235/236) activation in the cortex of *Mecp2*$^{+/-}$ mice with respect to WT littermates ($n = 5$, $P < 0.001$), whereas the activation of p-rpS6 (Ser240/244) was 41.9% less in female mutants than in control animals ($n = 5$, $P < 0.001$). Similarly, there was a reduction in activated rpS6 immunolocalization in the pyramidal cell layer of the CA1 area in the hippocampus of female mutants compared with WT controls (Fig. 8C; p-rpS6-Ser235/236: OD WT, 0.45 ± 0.02 and OD KO, 0.26 ± 0.03, $n = 5$, $P < 0.001$; p-rpS6-Ser240/244: OD WT, 0.38 ± 0.03 and OD KO, 0.21 ± 0.03, $n = 5$,

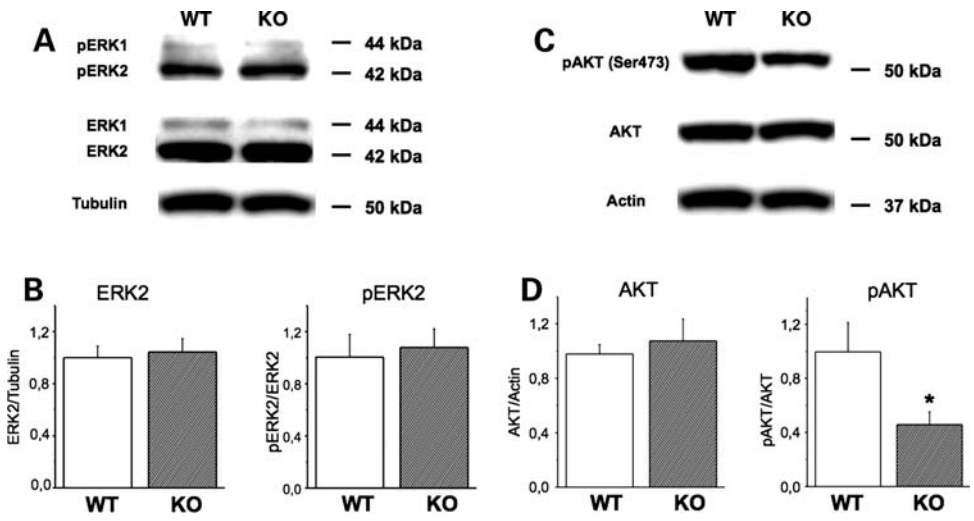

Figure 6. AKT phosphorylation is reduced in MeCP2$^{-/-}$ mouse brain. (**A**) Representative western blots (top) and summary data (bottom) showing pERK and total ERK in lysates from whole brain of MeCP2 KO and WT mice. Tubulin was included as a loading control. **(B)** Blot quantification showed that no change in pERK2 or total ERK2 was present in MeCP2 KO mice. Because of the extremely low levels of expression of ERK1, only ERK2 was analyzed. Error bars represent the standard error of the means. (**C**) Representative western blots showing pAKT and total AKT in whole-brain lysates from P56 MeCP2 KO and WT mice. Note that the phosphorylation of AKT at Ser473 is decreased in MeCP2 KO animals. (**D**) Blot quantitation showed that pAKT is clearly reduced in MeCP2 KO mice. No effect was present on total AKT levels. Error bars represent the standard error of the means. $^{*}P < 0.05$.

$P < 0.01$). No differences were found in total rpS6 expression in the two areas examined between the *Mecp2*$^{+/-}$ mutants and the WT mice (Fig. 7A–C; $P > 0.5$). These results indicate that altered levels of rpS6 activation can be found in an animal model of RTT closely resembling the human pathology.

MeCP2 non-cell autonomous effect on rpS6 phosphorylation

Finally, we assumed that if *Mecp2* loss impacts on such a complex signaling pathway, its deficiency might lead to non-cell autonomous effects. On the contrary, if deficits of rpS6 activation were produced by a completely cell-autonomous mechanism in heterozygous females only cells expressing the null allele would exhibit a phenotype. To test this hypothesis, we quantitatively analyzed p-rpS6 localization in the S1 cortex of *Mecp2* heterozygote females that show the mosaic expression of null and wild-type *Mecp2* alleles caused by the random inactivation of one X-linked *Mecp2* allele (44). Interestingly, the analysis of high magnification confocal images showed that p-rpS6 immunofluorescence was evidently reduced not only in MeCP2-negative neurons, but even in adjoining MeCP2 expressing cells (Fig. 8A). Indeed, the measurement of the mean p-rpS6 fluorescence intensity in the cell soma (Fig. 8B) revealed no differences between MeCP2^{+} and MeCP2^{-} neurons (p-rpS6-Ser235/236, MeCP2^{+} versus MeCP2^{-} cells, $n = 4$, $P > 0.3$; p-rpS6-Ser240/244, MeCP2^{+} versus MeCP2^{-} cells, $n = 4$, $P > 0.1$). Note that in MeCP2^{+} cortical neurons of *Mecp2* heterozygote females, the immunofluorescence signal for MeCP2 precisely co-localized with bright puncta of DAPI counterstain in the nucleus (Fig. 8C). This finding indicates that even a mosaic loss of MeCP2 in heterozygote female tissues might exert a more general impairment in signaling pathways and its downstream effectors.

DISCUSSION

In this study, we identified how the phosphorylation of rpS6 is broadly reduced across different brain areas and at different stages in mice lacking *Mecp2*. Surprisingly, this defect is detectable extremely early during post-natal development soon before neurological signs of the disease are evidently manifested. rpS6 abnormal low levels of phosphorylation are noticeable in both *Mecp2* null males and heterozygote females and the dynamic of its reduction follows the worsening of the neurological conditions. Therefore, p-rpS6 might represent a valuable biomarker of the disease onset and its development. This is particularly significant for RTT that currently lacks any reliable molecular marker to follow its neuropathological progression.

We observed that the phosphorylation of rpS6 is reduced in both MeCP2^{-} and MeCP2^{+} neurons in the brains of *Mecp2* heterozygous female. This finding suggests that rpS6 phospholevels in MeCP2 expressing cells are deregulated by the presence of neighboring *Mecp2* null neurons. This might be caused by the aberrant secretion from mutant neurons or glia cells of soluble factor(s) with neurotoxic effects. It might be hypothesized as well that the functional impairment of mutant neurons inhibits neuronal activity in adjoining cells therefore reducing rpS6 phosphorylation. Both possibilities are not alternative and can be simultaneously occurring at a different grade. Dysfunctions in non-cell autonomous pathways have been already proposed to contribute to RTT progression. In fact, *Mecp2* mutant astrocytes as well as microglia were found to induce multiple defects in WT neurons including the dendritic patterning, synapse formation and microtubule stability (45–48). However, our study indicated that p-rpS6 immunolabeling expression in glial cells is under the detection level of high-resolution confocal microscopy, thus suggesting that glia may not significantly contribute to the reduction in rpS6 phosphorylation in the brain of MeCP2 KO mice. The

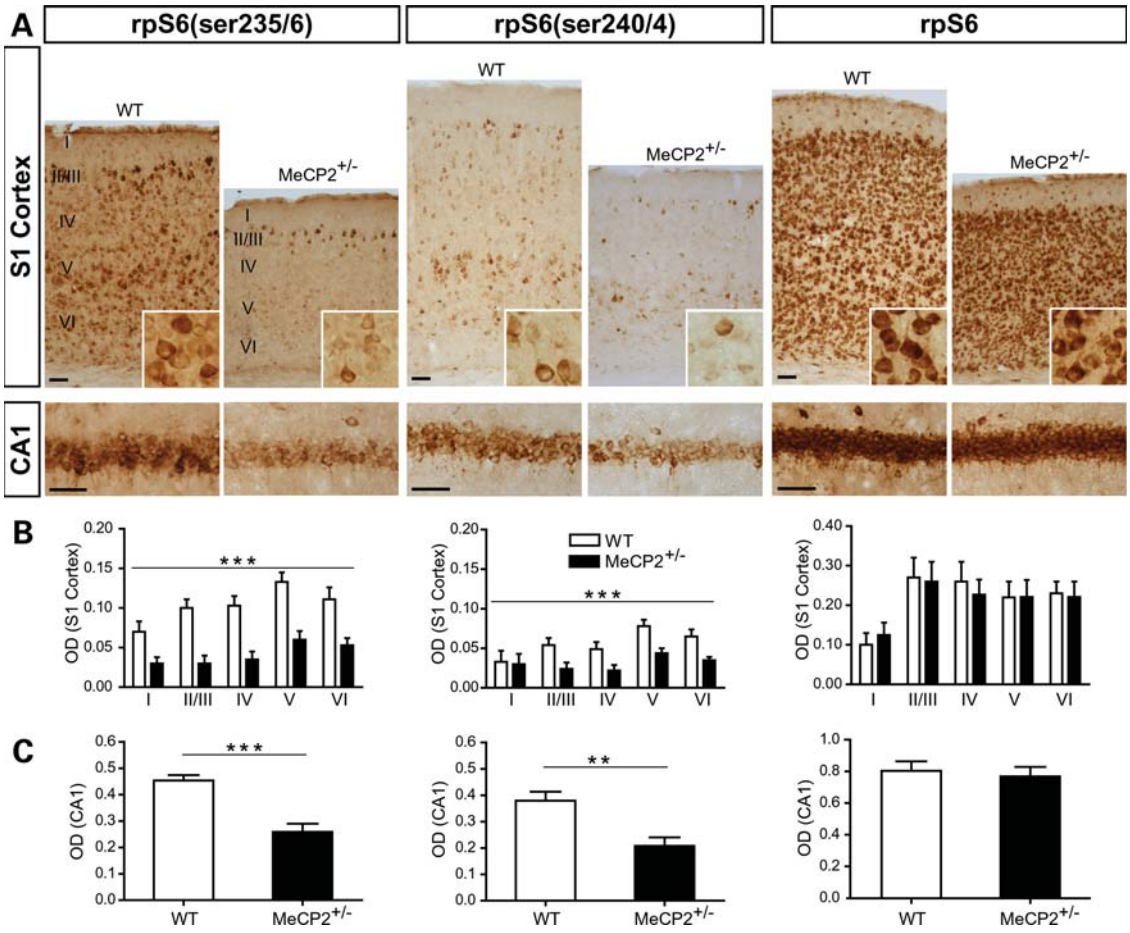

Figure 7. Activation of rpS6 is reduced in the brain of symptomatic MeCP2$^{+/-}$ female mice. (**A**) Immunohistochemical detection of p-rpS6 (Ser235/236), p-rpS6 (Ser240/244) and total rpS6 in the S1 cortex and in the CA1 area of the hippocampus in MeCP2$^{+/-}$ female mice and in WT controls at 10 months of age. Insets show higher magnification views of the immunolabeling pattern in layer V neurons of the S1 cortex. (**B** and **C**) Histograms show quantitative analysis of the labeling intensity of p-rpS6 and total rpS6 expression in layers I–VI of the S1 cortex as well as in the CA1 pyramidal cell layer of the hippocampus. The expression of p-rpS6 (Ser235/236) and p-rpS6 (Ser240/244) is significantly decreased in MeCP2$^{+/-}$ mice compared with WT controls in each cortical layer (B) as well as in the CA1 area of the hippocampus (C) compared with control animals. Total rpS6 immunostaining intensity is unchanged between genotypes in the two areas examined. Data are expressed as the mean ± SEM. $^{**}P < 0.01$, $^{***}P < 0.001$ (scale bars, 50 μm).

elucidation of non-cell autonomous molecular mechanisms acting in neuronal networks mosaic for the *Mecp2* mutation will be critical for our understanding of the disease pathogenesis in humans, which indeed affects primarily heterozygous girls.

Herein, we discovered a reduction in AKT/mTOR signaling associated with protein synthesis impairment in *Mecp2* mutant brains. To our knowledge, this is the first time that a cellular molecular cascade with pleiotropic functions in controlling cell homeostasis is found altered in RTT. These combined molecular defects might be responsible at least in part for the decreased number of excitatory hippocampal synapses described in mice lacking *Mecp2* (13,15,34–36). Nevertheless, RTT presents opposite molecular defects when compared with similar neurodevelopmental disorders, such as Fragile X, tuberous sclerosis and Pten-dependent autism, where, alternatively, mTOR signaling and protein synthesis result aberrantly up-regulated (49). Thus, RTT present peculiar molecular features where the hypoactivation of the mTOR signaling and limited protein synthesis is associated with reduced synaptic connectivity as already hypothesized by Kelleher and Bear (17). Despite the different molecular basis of RTT with respect to the other mentioned diseases, the final output is not so dissimilar, as in both cases, it causes a loss in neuronal network performance. In this scenario, the overall clinical neurological symptoms described as cognitive deficits, autism and impaired language and communication might arise from a positive as well as negative unbalance of the same molecular processes.

A large body of evidence indicates that the AKT/mTOR signaling pathway is a key modulator of the translation process, and its deficiency is frequently associated with defects in protein synthesis control (41,42,50). Consistent with this evidence, we identified a notable reduction in the overall translation rate in *Mecp2* mutant brains. This impairment was evident by analyzing the polysomal fraction of ribosomal profiling, whereas less significant in an *ex vivo* metabolic labeling system. This may be due to the different sensitivity/noise levels associated with the two different approaches. Alternatively, a deficit in protein turnover in the mutant brains might influence the final result of the metabolic labeling, while not affecting in any means the ribosomal profiling

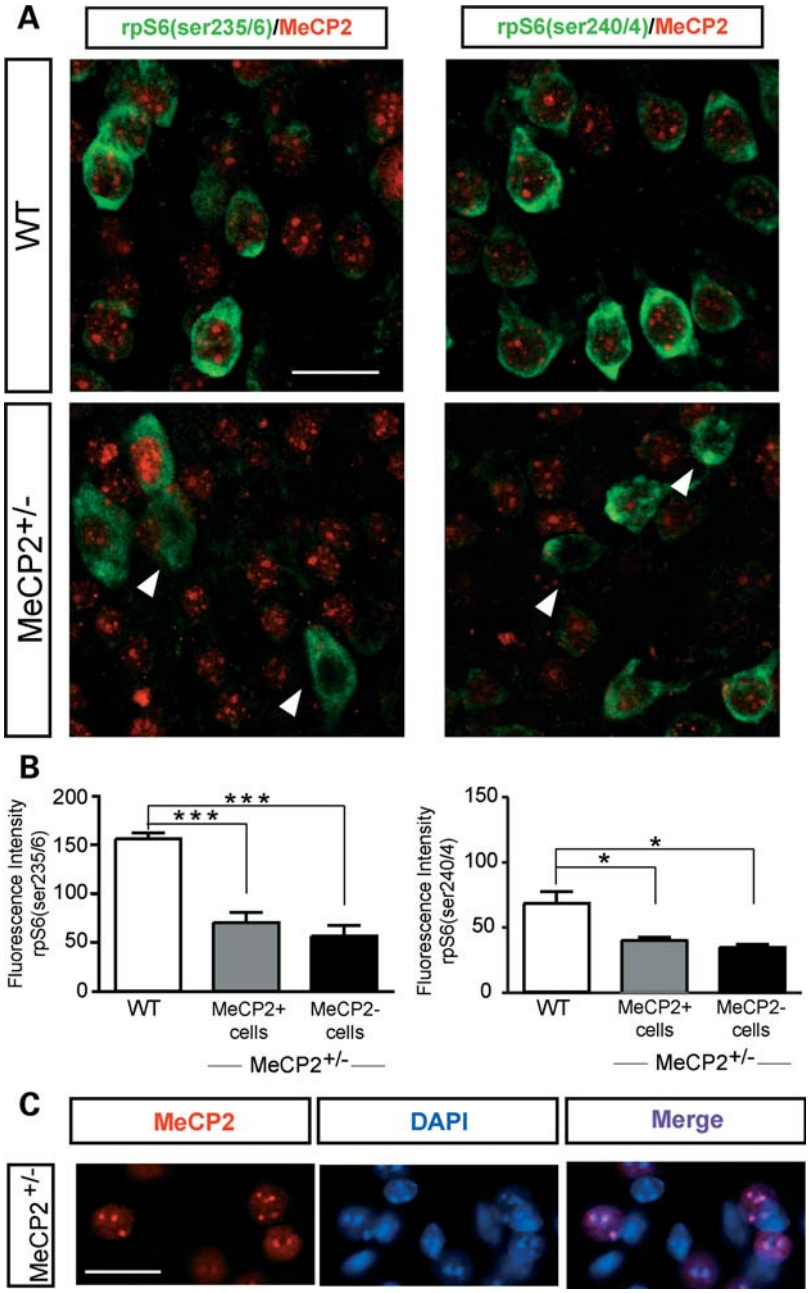

Figure 8. Alterations of rpS6 phosphorylation are non-cell autonomous in symptomatic MeCP2$^{+/-}$ female mutants. (**A**) Representative laser confocal images show double-immunofluorescence labeling for p-rpS6 (Ser235/236) or p-rpS6 (Ser240/244) (green) and MeCP2 (red) in layer V neurons of the S1 cortex of WT and MeCP2$^{+/-}$ mice. Neurons lacking MeCP2 immunoreactivity in female MeCP2$^{+/-}$ mice are indicated (arrowheads). Note that immunofluorescence signal for p-rpS6 (Ser235/236) and p-rpS6 (Ser240/244) is noticeable reduced in neurons of MeCP2$^{+/-}$ mice compared with WT. No obvious differences in staining intensity are detectable between MeCP2^{+} and MeCP2^{-} neurons in MeCP2$^{+/-}$ cortical sections. (**B**) Histograms show quantitatively that, compared with WT controls, there is a significant reduction in p-rpS6 (Ser235/236) and p-rpS6 (Ser240/244) immunofluorescence in MeCP2$^{+/-}$ mice that occurs with no statistically significant differences both in MeCP2^{+} and MeCP2^{-} cortical neurons. (**C**) Fluorescence image showing MeCP2 immunoreactivity in combination with DAPI counterstain in the S1 cortex of female MeCP2$^{+/-}$ mice. Data are expressed as the mean ± SEM. $^{*}P \leq 0.05$, $^{***}P \leq 0.001$ (scale bar, 20 μm).

which represents a snapshot of the initiation of translation. Future studies will investigate whether protein turnover is impaired in MeCP2 mutant brains.

Intriguingly, protein synthesis defects are occurring very early in RTT. Even if, at present, we cannot indicate whether this translational defect stands as a cause or an early effect of the disease, it is likely that it contributes to the overall progression of the disease. In this study, we did not address whether the rate of local protein synthesis is similarly affected. However, the reduction in mTOR activity is such pervasive in *Mecp2* mutant brains that is likely to impact on both global and local synthesis processes in comparable extent.

To determine whether translational repression in *Mecp2* mutants is affecting different transcripts with a similar

magnitude, we evaluated the effective amount of mRNAs on polysomes for non-directly related genes with a pivotal role in neuronal activity like CAMKIIα and PSD-95. Interestingly, we found that the polysomal incorporation of the two transcripts was significantly lower in *Mecp2* null mice with respect to WT. A similar trend was observed for Rack1, hnRNP A2/B1 and GADPH mRNAs. These three genes code for molecules that are not involved in neuronal activity and plasticity. Although restricted to the analysis of some genes, these results indicate that the translation impairment is not an event restricted to only few gene transcripts that impact to their protein production rate in similar levels.

On this basis, we favor the idea that a widespread limited protein production in *Mecp2* null neurons might restrain over time their metabolic activity and, ultimately, their excitability and plasticity.

Given that MeCP2 is a chromatin-associated transcriptional regulator, a large effort has been put in identifying the altered gene expression occurring in *Mecp2* mutant brains. However, a relative small amount of genes have been identified to be aberrantly expressed that do not account for fully explaining the development of the neuropathological signs (1,27,28). Why this is the case it remains still elusive. It has been proposed that the disease might be rooted in a genome-wide, but subtle, deregulation of global gene expression levels (51). Alternatively, the pathological gene alterations are strictly neuronal cell type specific and arduous to be identified in the expression profile studies conducted so far on entire brain subregions (52). Nevertheless, we described a new level of complexity of the disease represented by the widespread dysregulation of the protein synthesis process.

Considering our results, gene functional impairment in RTT might result from the sum of deregulated gene expression followed by a limited capability to produce the functional proteins.

Given the alterations that we discovered in two closely related processes like AKT/mTOR signaling and the protein synthesis rate, we suggest that a defect in this cellular pathway is responsible for the altered translational control in *Mecp2* mutant neurons. In contrast, we have not found any evidence for a direct role of MeCP2 in the ribosomal machinery controlling translational processes. This is also consistent with the subcellular localization of MeCP2 almost exclusively confined in the nucleus of differentiated neurons (11,44,53). Further, MeCP2 is excluded from nucleoli in the nuclear compartment where ribosomal genesis is mainly taking place (54,55) (S. Ricciardi and V. Broccoli, unpublished results). However, we cannot exclude that MeCP2 might regulate translation initiation by associating with components of the pre-initiation complex (56). This might be also consistent with the ability of MeCP2 to bind RNA and regulate its processing (57). This possibility warrants future investigations to be better delineated.

In conclusion, we identified the AKT/mTOR signaling as a molecular pathway down-regulated in *Mecp2* null neurons. Consistent with this finding, rpS6 phosphorylation is reduced in large areas of the *Mecp2* male null or female heterozygous brains providing an interesting biomarker for following the dynamics of the pathology. Finally, the general process of protein synthesis was found evidently impaired surprisingly even at early pre-symptomatic stage, making likely its contribution to the progression of the disease. Although our results revealed the translational control as an additional process altered by the pathological process; nevertheless, they provide a novel context where therapeutic interventions can be developed to successfully restrain or ameliorate the development of RTT.

MATERIALS AND METHODS

Animals

The experiments performed in this study were conducted in accordance with European Community Council Directive 86/609/EEC for care and use of experimental animals with protocols approved by the Italian Minister for Scientific Research. To obtain the litters of WT animals and *Mecp2* mutants used for this study, heterozygous *Mecp2*$^{tml.1Jae}$ mice with exon 3 deletion in *Mecp2* (8) were crossed to C57BL6 for one generation, followed by breeding among offspring and were maintained on a mixed background. Age-matched littermates were used in all experimental conditions to avoid possible consequences of genetic background unrelated to the *Mecp2* mutation (37).

Immunohistochemistry and immunofluorescence

Animals were anesthetized with an intraperitoneal injection of chloral hydrate and transcardially perfused with ice cold 4% paraformaldehyde in 0.1 M phosphate buffer (PB; pH 7.4). After perfusion, the brains were dissected and kept in the same fixative solution overnight at 4°C. After several washes in 0.1 M PB, the brains were then cryoprotected by immersion in 10, 20 and 30% sucrose solutions and subsequently cut in 30-μm sections with a cryostat. Cryosections were collected in phosphate-buffered saline (PBS, 0.01 M, pH 7.4) and processed for free-floating immunohistochemistry as described (58). After a blocking step in a PBS solution containing 0.05% Triton X-100 and 10% normal goat serum (NGS), sections were then incubated overnight at room temperature with the following primary antibodies: rabbit anti-phospho-rpS6 (Ser235/236) (1:100); rabbit anti-phospho-rpS6 (Ser240/244) (1:200); rabbit anti-rpS6 (1:100) from Cell Signaling Technology (Danvers, MA, USA). Antibodies were diluted in PBS with 3% NGS and 0.05 Triton X-100. Sections were then washed in PBS (4 × 10 min), incubated for 1 h with goat anti-rabbit biotinylated secondary antibodies (1:250; Vector Labs, Burlingame, CA, USA) diluted in 3% NGS and 0.05% Triton X-100 in PBS and transferred to a solution containing a biotin–avidin complex (1:100,Vector Labs). The peroxidase reaction product was visualized by incubation in a solution containing 3,3′-diaminobenzidine (0.05% in Tris–HCI, pH 7.6) with 0.01% H_2O_2 for 3 min. Sections were mounted on gelatin-coated glass slides and observed with a light microscope (Eclipse 800, Nikon, Japan) equipped with a CCD camera (Axiocam HRc, Zeiss, Germany).

Double immunofluorescence was performed with simultaneous addition of the primary antibodies as described (59). Briefly, cryosections were blocked in 10% normal donkey serum with 0.05% Triton X-100 in PBS for 1 h, then incubated at room temperature overnight with the following primary

antibodies: rabbit anti-phospho-rpS6 (Ser235/236) (1:100), rabbit anti-phospho-rpS6 (Ser240/244) (1:200), goat anti-MeCP2 (1:250, Santa Cruz Biotechnology, Santa Cruz, CA, USA), mouse anti-NeuN (1:100, Chemicon, Billerica, MA, USA) and mouse anti-GFAP (1:100, Cell Signaling Technology). After PBS washing, sections were incubated with secondary fluorescent antibodies (donkey anti-rabbit Alexa 488, Molecular Probes; donkey anti-goat Alexa 594, Invitrogen; donkey anti-mouse Alexa 594, Molecular Probes) for 1 h and, after several PBS rinses, incubated with DAPI (1:500, Invitrogen), mounted on gelatin-coated glass slides and observed with a confocal microscope (Zeiss LSM-5 Pascal, Germany).

Immunohistochemical data analysis

Total labeling of peroxidase in immunohistochemistry experiments was analyzed quantitatively by measuring OD on micrographs (10×) using a public-domain dedicated software (ImageJ, USA) by an operator blinded to the genotype. Measurements of OD in the cortex were obtained from 100 × 50 μm measuring boxes that were randomly placed in each cortical layer. OD values in the hippocampus were obtained from the CA1 pyramidal cell layer. Histograms illustrate the average OD obtained from three repeated measures in 4–5 sections per experimental animal at all ages examined (male WT $n = 3$; male MeCP2 KO $n = 3$; female WT $n = 5$; female MeCP2$^{+/-}$ $n = 5$). The mean OD of the corpus callosum was subtracted as background staining.

Double-fluorescence micrograph of the S1 cortex samples was acquired with a laser scanning confocal microscope, using the multitrack mode to avoid fluorescence crosstalk (pinhole: 1.0 airy unit). For the quantitative analysis of phospho-rpS6 fluorescence labeling in cortical neurons, Z-series stacks of four consecutive confocal sections (512 × 512 pixels) spaced by 2 μm were acquired at 20×. Images from both channels were overlaid and background labeling was subtracted. Fluorescence levels were analyzed on confocal images by measuring mean pixel intensity in either MeCP2-positive or MeCP2-negative neurons using ImageJ software. Histograms represent the mean fluorescence intensity calculated in at least 50 cortical neurons per animal (female WT $n = 4$; female MeCP2$^{+/-}$ $n = 4$). All data are presented as the mean ± SEM. Statistical analysis was done by Student's t-test as well as one- or two-way ANOVA using GraphPad Prism software (La Jolla, CA, USA). For presentation, digital micrographs were processed with the software ImageJ. Files were imported into Adobe Photoshop (Adobe Systems, San Jose, CA, USA), where images were cropped.

Polysomal profiles

Polysomal profiles were performed as described previously (60), with some modifications. Brain tissues were extracted from the skull and homogenized in 50 mM Tris–HCl (pH 7.4), 100 mM NaCl, 30 mM $MgCl_2$, 0.1% NP40, 100 μg/ml of cycloheximide, 40 U/ml of RNasin® and protease inhibitor cocktail (Sigma-Aldrich). Whole-brain extracts were clarified at 4°C for 10 min at 15 000*g*. The equivalent of 10 absorbance units at 254 nm were layered on a 15–50% sucrose gradient in 50 mM Tris–acetate, pH 7.5, 50 mM NH_4Cl, 12 mM $MgCl_2$ and 1 mM DTT and centrifuged at 4°C in a SW41Ti Beckman rotor for 3.5 h at 39 000 rpm. The absorbance at 254 nm was recorded by BioLogic LP software (Bio-Rad) and fractions were collected. In order to disrupt 80S ribosomes and polysomes, total extracts were treated with 30 mM EDTA for 10 min at 4°C. EDTA-treated and -untreated samples were then loaded on a sucrose gradient. Fractions were precipitated with 10% TCA (trichloroacetic acid) according to the standard protocol, separated on SDS–PAGE and analyzed by western blot. RNA was isolated from each fraction by phenol:chloroform:isoamilalcool (25:24:1) (Sigma-Aldrich) and mRNAs were analyzed by qRT-PCR. For quantitative measurements, polysomal profiles were scanned and the area of ribosomal peaks assessed with ImageJ (NIH) software.

Metabolic labeling

Six 400-μm sections were prepared from whole brain per animal (average age P40) using a tissue slicer. The slices were maintained in carbogenated, at 32.5°C ACSF (120 mM NaCl, 2.5 mM KCl, 1.2 mM $MgCl_2$, 2.5 mM $CaCl_2$, 26.2 mM $NaHCO_3$, 1 mM NaH_2PO_4, 11 mM Glucose) for 1.5 h. Following a 1.5 h recovery, slices were transferred to 15 mm diameter netwells (Corning) containing 5 ml of carbogenated ACSF. For each animal, three slices were incubated for 30 min in carbogenated ACSF with 100 μg/ml of cycloheximide. Slices were then incubated in carbogenated ACSF containing 11 μCi/ml of Promix ^{35}S-labeled methionine (Amersham) for 1 h. Netwells were then transferred to 12-well dish containing ice-cold dissection buffer to stop protein synthesis and remove the excess of ^{35}S-labeled methionine. Slices were subsequently removed and homogenized in ice-cold lysis buffer (50 mM Tris–HCl, pH 8.0, 150 mM NaCl, 1% NP40 and a mix of proteases inhibitors from Sigma-Aldrich). Extracts of 10 μl were TCA-precipitated on glass microfibre filters (Whatman) and counted. Obtained values were normalized by sample protein content, quantified using the bicinchoninic acid protein assay (Pierce). Final data were expressed as the ratio between the incorporated counts per minute (CPM) of non-treated slices and the CPM of cycloheximide-treated slices.

Western blotting

Brain tissues were extracted from the skull and homogenized in lysis buffer (50 mM Tris–HCl, pH 8.0, 150 mM NaCl, 1% NP40, 0.1% SDS and a mix of phosphatases and proteases inhibitors from Sigma-Aldrich) at 4°C. Lysates were clarified by centrifugation for 15 min at 18 000*g*, and protein concentration of the supernatant was determined using bovine serum albumin (BSA) as a standard (Bradford reagent assay, Sigma-Aldrich). Total lysates were boiled in SDS sample buffer, separated by SDS–PAGE and blotted to nitrocellulose membrane (Amersham). Filters were blocked in tris-buffered saline Tween-20 (0.1%) (TBST) (10 mM Tris–HCl, pH 8.0, 150 mM NaCl and 0.05% Tween-20) plus 5% BSA (Sigma-Aldrich) and incubated with primary antibodies for 16 h at 4°C. The following primary antibodies were used: rabbit polyclonal anti-MeCP2 (1:1000, Sigma-Aldrich),

rabbit polyclonal MeCP2 (1:1000, Lansberger's group), rabbit polyclonal anti-phospho-p70 S6K (Thr421/Ser424) (1:1000, Cell Signaling Technology), rabbit polyclonal anti-p70 S6K (1:1000, Cell Signaling Technology), rabbit polyclonal anti-phospho-mTOR (Ser2448) (1:1000, Cell Signaling Technology), rabbit monoclonal mTOR (1:1000, Cell Signaling Technology), rabbit polyclonal anti-phospo-AKT (Ser473) (1:1000, Cell Signaling Technology), mouse monoclonal anti-diphosphorylated ERK-1&2 (pERK) (1:1000, Sigma-Aldrich), mouse monoclonal anti-non-phosphorylated ERK-1&2 (1:1000, Sigma-Aldrich), mouse monoclonal anti-GADPH (1:5000, Millipore). After washing three times with TBST, filters were incubated with peroxidase-conjugated secondary antibodies (anti-mouse or rabbit IgG; 1:5000) (Amersham) for 1 h at room temperature. Detection was performed by enhanced chemiluminescence (EuroClone, Pero, Italy). For quantitative measurements, autoradiographs were scanned and signal intensity assessed with ImageJ (NIH) software.

Quantitative RT-PCR

An equal volume of RNA from each eleven-numbered fraction was reverse transcribed with random hexamer primers by Transcriptor High Fidelity cDNA Synthesis Kit (Roche), according to the manufacturer's instructions. Real-time PCR was performed with specific primers and SsoFast™ EvaGreen® Supermix (Bio-Rad) in a C1000™ Thermal Cycler (Bio-Rad). The amount of template and the number of amplification cycles were preliminarily optimized for each PCR to avoid conditions of saturation. For mRNA quantification, we constructed a standard curve with a serial dilution of RNA. For the experimental sample, the mRNA level was calculated using its standard curve obtained for that mRNA. The primer pairs used for the qRT-PCR were as follows: 5′-GTAACCCGTTGAACCCCATT-3′ (forward) and 5′-CC ATCCAATCGGTAGTAGCG-3′ (reverse) for 18S mRNA; 5′-GGACACCTGGATACCTCTCCC-3′ (forward) and 5′-GT ACAGGCGATGCTGGTCTT-3′ (reverse) for CAMKIIα mRNA; 5′-GTGGGCGGCGAGGATGGTGAA-3′ (forward) and 5′-CCGCCGTTTGCTGGGAATGAA-3′ (reverse) for PSD95 mRNA; 5′-AGGGCCACAATGGATGGGTA-3′ (forward) and 5′-TCTGGTCAGCTTCCACATGAT-3′ (reverse) for Rack1 mRNA; 5′-GGCTATAATGGGTATGG AGGAG-3′ (forward) and 5′-GGCATGGACTGTGGTCAT GA-3′ (reverse) for hnRNP A2/B1 mRNA; 5′-GGCAT GGACTGTGGTCATGA-3′ (forward) and 5′-TTCACCACC ATGGAGAAGC-3′ (reverse) for GADPH mRNA.

SUPPLEMENTARY MATERIAL

Supplementary Material is available at *HMG* online.

ACKNOWLEDGEMENTS

We gratefully acknowledge F. Bedogni, J.-C. Roux, L. Villard and M. Costa for fruitful discussion. We thank Federica Ungaro for technical assistance.

Conflict of Interest statement. None declared.

FUNDING

The authors are supported by the Italian Telethon Foundation (GGP07181 to V.B., GGP10032 to N.L., GGP09196 to T.P. and M.G.), the E-Rare EuroRett Consortium (to V.B., N.L., M.G. and T.P.), the FP7 projects Eurov1sion and Plasticise (T.P.) and the Compagnia San Paolo (S.B.). S.G. is a recipient of a Regione Piemonte fellowship.

REFERENCES

1. Bienvenu, T. and Chelly, J. (2006) Molecular genetics of Rett syndrome: when DNA methylation goes unrecognized. *Nat. Rev. Genet.*, **7**, 415–426.
2. Chahrour, M. and Zoghbi, H.Y. (2007) The story of Rett syndrome: from clinic to neurobiology. *Neuron*, **56**, 422–437.
3. Tao, J., Wu, H. and Sun, Y.E. (2009) Deciphering Rett syndrome with mouse genetics, epigenomics, and human neurons. *Int. Rev. Neurobiol.*, **89**, 147–160.
4. Hagberg, B. (2002) Clinical manifestations and stages of Rett syndrome. *Ment. Retard. Dev. Disabil. Res. Rev.*, **8**, 61–65.
5. Nan, X., Ng, H.H., Johnson, C.A., Laherty, C.D., Turner, B.M., Eisenman, R.N. and Bird, A. (1998) Transcriptional repression by the methyl-CpG-binding protein MeCP2 involves a histone deacetylase complex. *Nature*, **393**, 386–389.
6. Francke, U. (2006) Mechanisms of disease: neurogenetics of MeCP2 deficiency. *Nat. Clin. Pract. Neurol.*, **2**, 212–221.
7. Lasalle, J.M. and Yasui, D.H. (2009) Evolving role of MeCP2 in Rett syndrome and autism. *Epigenomics*, **1**, 119–130.
8. Chen, R.Z., Akbarian, S., Tudor, M. and Jaenisch, R. (2001) Deficiency of methyl-CpG binding protein-2 in CNS neurons results in a Rett-like phenotype in mice. *Nat. Genet.*, **27**, 327–331.
9. Guy, J., Hendrich, B., Holmes, M., Martin, J.E. and Bird, A. (2001) A mouse Mecp2-null mutation causes neurological symptoms that mimic Rett syndrome. *Nat. Genet.*, **27**, 322–326.
10. Dani, V.S., Chang, Q., Maffei, A., Turrigiano, G.G., Jaenisch, R. and Nelson, S.B. (2005) Reduced cortical activity due to a shift in the balance between excitation and inhibition in a mouse model of Rett syndrome. *Proc. Natl Acad. Sci. USA*, **102**, 12560–12565.
11. Kishi, N. and Macklis, J.D. (2005) Dissecting MECP2 function in the central nervous system. *J. Child Neurol.*, **20**, 753–759.
12. Moretti, P. and Zoghbi, H.Y. (2006) MeCP2 dysfunction in Rett syndrome and related disorders. *Curr. Opin. Genet. Dev.*, **16**, 276–281.
13. Chao, H.T., Zoghbi, H.Y. and Rosenmund, C. (2007) MeCP2 controls excitatory synaptic strength by regulating glutamatergic synapse number. *Neuron*, **56**, 58–65.
14. Monteggia, L.M. and Kavalali, E.T. (2009) Rett syndrome and the impact of MeCP2 associated transcriptional mechanisms on neurotransmission. *Biol. Psychiatry*, **65**, 204–210.
15. Tropea, D., Giacometti, E., Wilson, N.R., Beard, C., McCurry, C., Fu, D.D., Flannery, R., Jaenisch, R. and Sur, M. (2009) Partial reversal of Rett syndrome-like symptoms in MeCP2 mutant mice. *Proc. Natl Acad. Sci. USA*, **106**, 2029–2034.
16. Boggio, E.M., Lonetti, G., Pizzorusso, T. and Giustetto, M. (2010) Synaptic determinants of Rett syndrome. *Front. Syn. Neurosci.*, **2**, 1–12.
17. Kelleher, R.J. III and Bear, M.F. (2008) The autistic neuron: troubled translation? *Cell*, **135**, 401–406.
18. Bourgeron, T. (2009) A synaptic trek to autism. *Curr. Opin. Neurobiol.*, **19**, 231–234.
19. Krab, L.C., Goorden, S.M. and Elgersma, Y. (2008) Oncogenes on my mind: ERK and MTOR signaling in cognitive diseases. *Trends Genet.*, **24**, 498–510.
20. Hoeffer, C.A. and Klann, E. (2010) mTOR signaling: at the crossroads of plasticity, memory and disease. *Trends Neurosci.*, **33**, 67–75.
21. Bear, M.F., Dölen, G., Osterweil, E. and Nagarajan, N. (2008) Fragile X: translation in action. *Neuropsychopharmacology*, **33**, 84–87.
22. Ehninger, D., Han, S., Shilyansky, C., Zhou, Y., Li, W., Kwiatkowski, D.J., Ramesh, V. and Silva, A.J. (2008) Reversal of learning deficits in a Tsc2+/− mouse model of tuberous sclerosis. *Nat. Med.*, **14**, 843–848.
23. Schmidt, H., Ker, W., Giese, R., Hallschmid, M. and Enders, A. (2009) Intranasal insulin to improve developmental delay in children with 22q13

deletion syndrome: an exploratory clinical trial. *J. Med. Genet.*, **46**, 217–222.
24. Kelleher, R.J. 3rd, Govindarajan, A. and Tonegawa, S. (2004) Translational regulatory mechanisms in persistent forms of synaptic plasticity. *Neuron*, **44**, 59–73.
25. Jaworski, J. and Sheng, M. (2006) The growing role of mTOR in neuronal development and plasticity. *Mol. Neurobiol.*, **34**, 205–219.
26. Richter, J.D. and Klann, E. (2009) Making synaptic plasticity and memory last: mechanisms of translational regulation. *Genes Dev.*, **23**, 1–11.
27. Jordan, C., Li, H.H., Kwan, H.C. and Francke, U. (2007) Cerebellar gene expression profiles of mouse models for Rett syndrome reveal novel MeCP2 targets. *BMC Med. Genet.*, **8**, 36.
28. Urdinguio, R.G., Lopez-Serra, L., Lopez-Nieva, P., Alaminos, M., Diaz-Uriarte, R., Fernandez, A.F. and Esteller, M. (2008) Mecp2-null mice provide new neuronal targets for Rett syndrome. *PLoS One*, **3**, e3669.
29. Pende, M., Um, S.H., Mieulet, V., Sticker, M., Goss, V.L., Mestan, J., Mueller, M., Fumagalli, S., Kozma, S.C. and Thomas, G. (2004) S6K1(-/-)/S6K2(-/-) mice exhibit perinatal lethality and rapamycin-sensitive 5′-terminal oligopyrimidine mRNA translation and reveal a mitogen-activated protein kinase-dependent S6 kinase pathway. *Mol. Cell. Biol.*, **243**, 112–124.
30. Ruvinsky, I. and Meyuhas, O. (2006) Ribosomal protein S6 phosphorylation: from protein synthesis to cell size. *Trends Biochem. Sci.*, **31**, 342–348.
31. Roux, P.P. *et al.* (2007) RAS/ERK signaling promotes site-specific ribosomal protein S6 phosphorylation via RSK and stimulates cap-dependent translation. *J. Biol. Chem.*, **282**, 14056–1464.
32. Banko, J.L., Hou, L. and Klann, E. (2004) NMDA receptor activation results in PKA- and ERK-dependent Mnk1 activation and increased eIF4E phosphorylation in hippocampal area CA1. *J. Neurochem.*, **91**, 462–470.
33. Banko, J.L., Hou, L., Poulin, F., Sonenberg, N. and Klann, E. (2006) Regulation of eukaryotic initiation factor 4E by converging signaling pathways during metabotropic glutamate receptor-dependent long-term depression. *J. Neurosci.*, **26**, 2167–2173.
34. Fukuda, T., Itoh, M., Ichikawa, T., Washiyama, K. and Goto, Y. (2005) Delayed maturation of neuronal architecture and synaptogenesis in cerebral cortex of Mecp2-deficient mice. *J. Neuropathol. Exp. Neurol.*, **64**, 537–544.
35. Belichenko, N.P., Belichenko, P.V. and Mobley, W.C. (2009a) Evidence for both neuronal cell autonomous and nonautonomous effects of methyl-CpG-binding protein 2 in the cerebral cortex of female mice with Mecp2 mutation. *Neurobiol. Dis.*, **34**, 71–77.
36. Belichenko, P.V., Wright, E.E., Belichenko, N.P., Masliah, E., Li, H.H., Mobley, W.C. and Francke, U. (2009b) Widespread changes in dendritic and axonal morphology in Mecp2-mutant mouse models of Rett syndrome: evidence for disruption of neuronal networks. *J. Comp. Neurol.*, **514**, 240–258.
37. Lonetti, G., Angelucci, A., Morando, L., Boggio, E.M., Giustetto, M. and Pizzorusso, T. (2010) Early environmental enrichment moderates the behavioral and synaptic phenotype of MeCP2 null mice. *Biol. Psychiatry*, **67**, 657–665.
38. Ballas, N., Lioy, D.T., Grunseich, C. and Mandel, G. (2009) Non-cell autonomous influence of MeCP2 deficient glia on neuronal dendritic morphology. *Nat. Neurosci.*, **12**, 311–317.
39. Grosso, S., Volta, V., Sala, L.A., Vietri, M., Marchisio, P.C., Ron, D. and Biffo, S. (2008) PKCbetaII modulates translation independently from mTOR and through RACK1. *Biochem. J.*, **415**, 77–85.
40. Dufner, A. and Thomas, G. (1999) Ribosomal S6 kinase signaling and the control of translation. *Exp. Cell Res.*, **253**, 100–109.
41. Hay, N. and Sonenberg, N. (2004) Upstream and downstream of mTOR. *Genes Dev.*, **18**, 1926–1945.
42. Ma, X.M. and Blenis, J. (2009) Molecular mechanisms of mTOR-mediated translational control. *Nat. Rev. Mol. Cell Biol.*, **10**, 307–318.
43. Sarbassov, D.D., Guertin, D.A., Ali, S.M. and Sabatini, D.M. (2005) Phosphorylation and regulation of Akt/PKB by the rictor-mTOR complex. *Science*, **307**, 1098–1101.
44. LaSalle, J., Goldstine, J., Balmer, D. and Greco, C. (2001) Quantitative localization of heterologous methyl-CpG-binding protein 2 (MeCP2) expression phenotypes in normal and Rett syndrome brain by laser scanning cytometry. *Hum. Mol. Genet.*, **10**, 1729–1740.
45. Ballas, N., Lioy, D.T., Grunseich, C. and Mandel, G. (2209) Non-cell autonomous influence of MeCP2-deficient glia on neuronal dendritic morphology. *Nat. Neurosci.*, **12**, 311–317.
46. Maezawa, I., Swanberg, S., Harvey, D., LaSalle, J.M. and Jin, L.W. (2009) Rett syndrome astrocytes are abnormal and spread MeCP2 deficiency through gap junctions. *J. Neurosci.*, **29**, 5051–5061.
47. Zoghbi, H.Y. (2009) Rett syndrome: what do we know for sure? *Nat. Neurosci.*, **12**, 239–240.
48. Maezawa, I. and Jin, L.W. (2010) Rett syndrome microglia damage dendrites and synapses by the elevated release of glutamate. *J. Neurosci.*, **30**, 5346–5356.
49. Costa-Mattioli, M., Sossin, W.S., Klann, E. and Sonenberg, N. (2009) Translational control of long-lasting synaptic plasticity and memory. *Neuron*, **61**, 10–26.
50. Laplante, M. and Sabatini, D.M. (2009) mTOR signaling at a glance. *J. Cell Sci.*, **122**, 3589–3594.
51. Skene, P.J., Illingworth, R.S., Webb, S., Kerr, A.R., James, K.D., Turner, D.J., Andrews, R. and Bird, A.P. (2010) Neuronal MeCP2 is expressed at near histone-octamer levels and globally alters the chromatin state. *Mol. Cell.*, **37**, 457–468.
52. Fyffe, S.L., Neul, J.L., Samaco, R.C., Chao, H.T., Ben-Shachar, S., Moretti, P., McGill, B.E., Goulding, E.H., Sullivan, E., Tecott, L.H. *et al.* (2008) Deletion of Mecp2 in Sim1-expressing neurons reveals a critical role for MeCP2 in feeding behavior, aggression, and the response to stress. *Neuron*, **59**, 947–958.
53. Shahbazian, M.D., Antalffy, B., Armstrong, D.L. and Zoghbi, H.Y. (2002) Insight into Rett syndrome: MeCP2 levels display tissue- and cell- specific differences and correlate with neuronal maturation. *Hum. Mol. Genet.*, **11**, 115–124.
54. Thatcher, K.N. and LaSalle, J.M. (2006) Dynamic changes in Histone H3 lysine 9 acetylation localization patterns during neuronal maturation require MeCP2. *Epigenetics*, **1**, 24–31.
55. Marchi, M., Guarda, A., Bergo, A., Landsberger, N., Kilstrup-Nielsen, C., Ratto, G.M. and Costa, M. (2007) Spatio-temporal dynamics and localization of MeCP2 and pathological mutants in living cells. *Epigenetics*, **2**, 187–197.
56. Sonenberg, N. and Hinnebusch, A.G. (2009) Regulation of translation initiation in eukaryotes: mechanisms and biological targets. *Cell*, **136**, 731–745.
57. Young, J.I., Hong, E.P., Castle, J.C., Crespo-Barreto, J., Bowman, A.B., Rose, M.F., Kang, D., Richman, R., Johnson, J.M., Berget, S. *et al.* (2005) Regulation of RNA splicing by the methylation-dependent transcriptional repressor methyl-CpG binding protein 2. *Proc. Natl Acad. Sci. USA*, **102**, 17551–17558.
58. Boggio, E.M., Putignano, E., Sassoe-Pognetto, M., Pizzorusso, T. and Giustetto, M. (2007) Visual stimulation activates ERK in synaptic and somatic compartments of rat cortical neurons with parallel kinetics. *PLoS One*, **2**, e604.
59. Vara, H., Onofri, F., Benfenati, F., Sassoè-Pognetto, M. and Giustetto, M. (2009) ERK activation in axonal varicosities modulates presynaptic plasticity in the CA3 region of the hippocampus through synapsin I. *Proc. Natl Acad. Sci. USA*, **106**, 9872–9877.
60. Ceci, M., Gaviraghi, C., Gorrini, C., Sala, L.A., Offenhäuser, N., Marchisio, P.C. and Biffo, S. (2003) Release of eIF6 (p27BBP) from the 60S subunit allows 80S ribosome assembly. *Nature*, **426**, 579–584.
61. Kishi, N. and Macklis, J.D. (2004) MECP2 is progressively expressed in post-migratory neurons and is involved in neuronal maturation rather than cell fate decisions. *Mol. Cell. Neurosci.*, **27**, 306–321.